Grant No. AF-AFOSR-1-63
Project No. 9781-01

LAMINAR, TRANSITIONAL, AND TURBULENT HEAT TRANSFER AFTER A SHARP DISCONTINUITY

by

VICTOR ZAKKAY, KAORU TOBA, and TA-JIN KUO

JULY 1963

POLYTECHNIC INSTITUTE OF BROOKLYN

DEPARTMENT
of
AEROSPACE ENGINEERING
and
APPLIED MECHANICS

PIBAL REPORT NO. 771

LAMINAR, TRANSITIONAL, AND TURBULENT HEAT TRANSFER AFTER A SHARP DISCONTINUITY

by

Victor Zakkay, Kaoru Toba, and Ta-Jin Kuo

The study was supported by the
Air Force Office of Scientific Research
Grant No. AF-AFOSR-1-63.

Polytechnic Institute of Brooklyn

Department

of

Aerospace Engineering and Applied Mechanics

July 1963

PIBAL Report No. 771

LAMINAR, TRANSITIONAL, AND TURBULENT HEAT TRANSFER AFTER A SHARP DISCONTINUITY[†]

by

Victor Zakkay[*], Kaoru Toba[**], and Ta-Jin Kuo[***]

Polytechnic Institute of Brooklyn

SUMMARY

A flow model has been previously developed for treating the boundary layer characteristics downstream of a surface discontinuity. The flow field in the neighborhood of the discontinuity or a sharp corner is divided into two regions: The flow upstream of the discontinuity which is obtained by standard techniques, and that of downstream which is obtained by expanding both the supersonic and subsonic flow fields upstream of the discontinuity inviscidly around the corner. Downstream of the discontinuity, the flow is represented by a viscous nonsimilar sublayer which starts at the discontinuity, and by a viscous shear layer which has the profiles immediately downstream of the discontinuity as initial conditions. Based upon this flow

---

[†]The study was supported by the Air Force Office of Scientific Research Grant No. AF-AFOSR-1-63.

[*]Research Associate Professor, Aerospace Engineering

[**]Research Associate, presently at Douglas Aircraft Co., Los Angeles, California

[***]Graduate Assistant

model, analysis has been developed using the inner and outer expansion techniques.

It is the purpose of this report to improve on the treatment of the laminar analysis, and to extend the technique of application of this model to include turbulent and transitional flow downstream of the corner. Finally, the results are compared with some of the experimental data available in the literature. It is indicated that good agreement was obtained.

TABLE OF CONTENTS

LIST OF ILLUSTRATIONS

LIST OF TABLES

LIST OF SYMBOLS

A	constant defined in Eq. (4)
c	constant = $\rho\mu$
c_f	skin friction coefficient
$c(n)$	constants tabulated in reference 9
C_1	constant defined in Eq. (6)
D	constant defined in Eq. (33)
$f_0(\eta), f_{\frac{1}{2}}(\eta), f_{\frac{1}{2}\frac{1}{2}}(\eta), f_1(\eta)$	functions of η defined in Eq. (7) [see Tables 1, 3, 4]
$g_0(\eta), g_1(\eta)$	functions of η defined in Eq. (8) [see Table 2]
h	enthalpy
H	total enthalpy
$k_{\frac{1}{2}}, k_1$	constants defined in Eqs. (4) and (5)
M	Mach number
n	positive integer (= 7, 8, 9, 10)
Nu	Nusselt number
p	pressure
Pr	Prandtl number
q	amount of heat transferred at the wall per unit time and unit area
Re_s	Reynolds number defined by $\rho_{se}\sqrt{H_{ei}}R_o/\mu_{se}$
R_o	reference length
s	$\int_0^x \rho_{ei}\mu_{ei}u_e dx$
St	Stanton number

LIST OF SYMBOLS (Contd)

u, U	velocity components in x-direction
v	velocity component in y-direction
x, y	Cartesian coordinates
δ	thickness of shear layer (or boundary layer)
Δ	reference thickness of boundary layer
η	variable defined in Eq. (3)
θ	momentum thickness
$\varkappa$	coefficient of heat conduction
μ	coefficient of viscosity
ν	coefficient of kinematic viscosity
ρ	density
σ	measure of vorticity gradient defined in Eq. (1)
τ	variable defined in Eq. (2)
Φ	measure of curvature of enthalpy profile defined in Eq. (1)
ψ	stream function
ω	measure of vorticity defined in Eq. (1)
Ω	measure of slope in enthalpy profile defined in Eq. (1)

Subscripts

ei	condition external to shear layer
se	stagnation condition after normal shock
*	reference state

SECTION I

INTRODUCTION

In many practical problems in hypersonic flight, bodies having surface discontinuities or regions with rapid variation of curvature are used. Typical bodies of such type are, for example, cone-cylinder combinations.

A sublayer model for the boundary layer characteristics downstream of the corner was first introduced by Sternberg[1]. In Sternberg's paper, the predicted boundary layer characteristics are compared with measurements of the recovery factor. At a later date, independently, Zakkay and Tani[2] reintroduced the same model and presented a detailed method for evaluating the development of shear layer and sublayer as well as the heat transfer rate when the oncoming boundary layer is laminar. These analyses were made by using an expansion technique similar to that used by Görtler. In the present work, the above technique is extended to include both transitional and turbulent boundary layers. Again in this case, the method chosen for analyzing the boundary layer characteristics is based on the model introduced in reference 1.

According to the sublayer model, the flow field of interest may be divided into two layers, an inner nonsimilar layer starting at the corner, and an outer shear layer. The initial conditions for the shear layer are obtained by the inviscid and adiabatic expansion of the boundary layer profiles ahead of the corner. The new viscous layer is shown in

Fig. 1 and will be referred to as sublayer since it underlies the outer shear layer. Distinction should be made between the proposed sublayer and the one usually associated with turbulent flow.

This flow model presupposes that the initial velocity profile of the shear layer is very steep. In effect, the flow field downstream of the corner will be considered the same as that which would exist over a flat plate, with oncoming viscous flow having shear and shear gradient. Consequently, the corner itself is treated as a singularity similar to the leading edge of a flat plate. Hence, the problem is similar to the one treated by Li[3] and Glauert[4]. However, in this case, the analysis uses the experimental pressure distribution and will not be concerned with the higher order effects such as the induced pressure gradient.

When the boundary layer flow is fully turbulent up to the corner, the sublayer model is expected to become more effective, since the velocity profile is steeper than the one obtained for laminar flow.

Mathematical treatment, however, is not developed rigorously because of the new unknowns, i.e., Reynolds stress and turbulent heat flux. Moreover, according to the equivalence of the flow field to a flow over a flat plate placed in a turbulent oncoming flow, the flow represented by the sublayer may be laminar close to the corner and may undergo the transition to turbulence somewhere downstream. Four independent sets of experimental data presented show that the observed heat transfer rate has such a trend. Taking into account such a phenomenon, the sublayer plus simple mass flow consideration gives good results of heat transfer rate near the corner and somewhat downstream of the corner where the state of affairs becomes asymptotic.

Fig. 1 and will be referred to as sublayer since it underlies the outer shear layer. Distinction should be made between the proposed sublayer and the one usually associated with turbulent flow.

This flow model presupposes that the initial velocity profile of the shear layer is very steep. In effect, the flow field downstream of the corner will be considered the same as that which would exist over a flat plate, with oncoming viscous flow having shear and shear gradient. Consequently, the corner itself is treated as a singularity similar to the leading edge of a flat plate. Hence, the problem is similar to the one treated by Li[3] and Glauert[4]. However, in this case, the analysis uses the experimental pressure distribution and will not be concerned with the higher order effects such as the induced pressure gradient.

When the boundary layer flow is fully turbulent up to the corner, the sublayer model is expected to become more effective, since the velocity profile is steeper than the one obtained for laminar flow.

Mathematical treatment, however, is not developed rigorously because of the new unknowns, i.e., Reynolds stress and turbulent heat flux. Moreover, according to the equivalence of the flow field to a flow over a flat plate placed in a turbulent oncoming flow, the flow represented by the sublayer may be laminar close to the corner and may undergo the transition to turbulence somewhere downstream. Four independent sets of experimental data presented show that the observed heat transfer rate has such a trend. Taking into account such a phenomenon, the sublayer plus simple mass flow consideration gives good results of heat transfer rate near the corner and somewhat downstream of the corner where the state of affairs becomes asymptotic.

$$\eta = \frac{u_e}{(2s)^{\frac{1}{2}}} \int_o^y \rho dy \tag{3}$$

Development of the shear layer in the neighborhood of $s = 0$ is determined by expanding the stream function in power series of $s^{\frac{1}{2}}$ and integrating the momentum and energy equations. The results, expressed in terms of η, are

$$u = u_o\Big[1 + (2s)^{\frac{1}{2}}\,\omega\Big(\frac{1}{u_e\delta_1}\,\eta + \frac{k_{\frac{1}{2}}}{\sqrt{2}}\Big) + s\,\Big\{2\sigma\Big(\frac{1}{\delta_1^2 u_e^2}\,\eta^2 + k_{\frac{1}{2}}\,\frac{\sqrt{2}}{u_e\delta_1}\,\eta + \frac{k_{\frac{1}{2}}^2}{2} + \frac{1}{u_o u_e \delta_1^2}\Big) + k_1\omega - \frac{p_1 A}{\rho_{ei} c u_e u_o}\Big\} + O(s^{\frac{3}{2}})\Big] \tag{4}$$

$$H = h_o\Big[1 + (2s)^{\frac{1}{2}}\,\Omega\Big(\frac{1}{u_e\delta_1}\,\eta + \frac{k_{\frac{1}{2}}}{\sqrt{2}}\Big) + s\,\Big\{2\Phi\Big(\frac{1}{\delta_1^2 u_e^2}\,\eta^2 + k_{\frac{1}{2}}\,\frac{\sqrt{2}}{u_e\delta_1}\,\eta + \frac{k_{\frac{1}{2}}^2}{2} + \frac{1}{u_o u_e \delta_1^2}\Big) + k_1\Omega + O(s^{\frac{3}{2}})\Big] \tag{5}$$

where $A = \frac{1}{u_o h_{ei}}\,(h_o - \frac{u_o^2}{2})$ and $k_{\frac{1}{2}}$, k_1 are constants. It is observed that if $p_1 = 0$ one can expect Crocco relation between the two profiles to hold. In fact, then one can also expect the same relation for the initial profiles, namely, with a constant C_1, one gets

$$\left.\begin{aligned} C_1 u_o + h_w &= h_o \\ C_1 u_o \omega &= h_o \Omega \\ C_1 u_o \sigma &= h_o \Phi \end{aligned}\right\}, \tag{6}$$

By these relations Eq. (5) immediately follows from Eq. (4).

For the sublayer, the stream function and the enthalpy are expanded as follows:

$$\psi(s,\eta) = (2s)^{\frac{1}{2}}\left[f_o(\eta) + s^{\frac{1}{2}}\beta_{\frac{1}{2}} f_{\frac{1}{2}}(\eta) + s\left\{\beta_{\frac{1}{2}}^2 f_{\frac{1}{2}\frac{1}{2}}(\eta) + \beta_1 f_1(\eta)\right\} + \cdots\right] \tag{7}$$

$$\begin{aligned} H(s,\eta) = h_w + H_e\Big[&\gamma_o g_o(\eta) + s^{\frac{1}{2}}\left\{\beta_{\frac{1}{2}}\gamma_o f_{\frac{1}{2}}'(\eta) + \gamma_{\frac{1}{2}} g_{\frac{1}{2}}(\eta)\right\} \\ &+ s\left\{\beta_{\frac{1}{2}}^2\gamma_o f_{\frac{1}{2}\frac{1}{2}}'(\eta) + \varepsilon_1 g_1(\eta)\right\} + \cdots\Big] \end{aligned} \tag{8}$$

where $\beta_{\frac{1}{2}}$, β_1, ..., γ_o, $\gamma_{\frac{1}{2}}$, ε_1, ... are constants and H_e is a reference enthalpy. These expressions are substituted into the governing differential equations and the coefficients of the same power of s are equated to zero. Thus, one arrives at a set of differential equations for f_o, $f_{\frac{1}{2}}$, etc. The boundary conditions at the wall are the no-slip and the constant temperature ($H = h_w$). The outer boundary conditions are found by matching the profiles with those given by Eqs. (4) and (5) at the edge of the sublayer. Thus the following sets of differential equations are obtained:

$$\left.\begin{aligned} u_e &= u_o \\ f_o''' + f_o f_o'' &= 0 \\ f_o(0) = f_o'(0) &= 0 \quad , \quad f_o' \to 1 \text{ as } \eta \to \infty \end{aligned}\right\} \tag{9}$$

$$\gamma_o = \frac{h_o - h_w}{H_e} \quad , \quad \beta_{\frac{1}{2}} = \sqrt{2}\ \frac{w}{u_e \delta_1}$$

$$\left.\begin{aligned} g_o'' + f_o g_o' &= 0 \\ g_o(0) = 0 \ , \ g_o &\to 1 \ \text{ as } \ \eta \to \infty \end{aligned}\right\} \qquad (10)$$

Upon comparing Eqs. (9) and (10) there results a relation $g_o = f_o'$. Furthermore,

$$\left.\begin{aligned} \gamma_{\frac{1}{2}} = \frac{\sqrt{2}}{H_e u_e \delta_1} [h_o \Omega - (h_o - h_w)\omega] \ , \ k_{\frac{1}{2}} &= -\frac{\sqrt{2}}{u_e \delta_1} \beta \\ f_{\frac{1}{2}}'' + f_o f_{\frac{1}{2}}' - f_o' f_{\frac{1}{2}} + 2 f_o'' f_{\frac{1}{2}} &= 0 \\ f_{\frac{1}{2}}(0) = f_{\frac{1}{2}}'(0) = 0 \ , \ f_{\frac{1}{2}}'(\eta) &\to \eta - \beta \ \text{ as } \ \eta \to \infty \end{aligned}\right\} \qquad (11)$$

$$\left.\begin{aligned} g_{\frac{1}{2}}'' + f_o g_{\frac{1}{2}}' - f_o' g_{\frac{1}{2}} &= 0 \\ g_{\frac{1}{2}}(0) = 0 \ , \ g_{\frac{1}{2}}(\eta) &\to \eta - \beta \ \text{ as } \ \eta \to \infty \end{aligned}\right\} \qquad (12)$$

$$\left.\begin{aligned} \beta_1 &= \frac{2\sigma}{u_e^2 \delta_1} \\ f_1''' + f_o f_1'' - 2 f_o' f_1' + 3 f_o'' f_1 &= 0 \\ f_1(0) = f_1'(0) &= 0 \\ f_1'(\eta) &\to \eta^2 - 2\beta\eta + \beta^2 + 1 \ \text{ as } \ \eta \to \infty \end{aligned}\right\} \qquad (13)$$

$$k_1 = \frac{\omega}{u_e^2 \delta_1} K = \frac{\omega}{u_e^2 \delta_1} \left[(2E - \beta^2) + \frac{p_1 \delta_1^2}{c \rho_{ei} u_e} \frac{1}{\omega^2} \left\{ \frac{h_o}{h_{ei}} - \frac{u_o^2}{2h_{ei}} - B(\infty) \frac{\rho_{ei}}{\rho_w} \right\} \right]$$

$$f_{\frac{1}{2}\frac{1}{2}}''' + f_o f_{\frac{1}{2}\frac{1}{2}}'' - 2f_o' f_{\frac{1}{2}\frac{1}{2}}' + 3f_o'' f_{\frac{1}{2}\frac{1}{2}} - f_{\frac{1}{2}}'^2 + 2f_{\frac{1}{2}} f_{\frac{1}{2}}''$$

$$= \frac{1}{\beta_{\frac{1}{2}}^2} \frac{2p_1}{c u_e^3 \rho_w} \left[1 + \frac{(h_o - h_w)}{h_w} f_o' - \frac{u_e^2}{2h_w} f_o'^2 \right] \qquad (14)$$

$$f_{\frac{1}{2}\frac{1}{2}}(0) = f_{\frac{1}{2}\frac{1}{2}}'(0) = 0$$

$$f_{\frac{1}{2}\frac{1}{2}}'(\eta) \to \frac{1}{2} \left[K - \frac{p_1 \delta_1^2}{c \rho_{ei} u_o} \frac{1}{\omega^2} \left\{ \frac{h_o}{h_{ei}} - \frac{u_o^2}{2h_{ei}} \right\} \right] \text{ as } \eta \to \infty$$

where E is a constant to be determined by the behavior of $f_{\frac{1}{2}}$ such that

$$f_{\frac{1}{2}}(\eta) \to \frac{\eta^2}{2} - \beta\eta + E \quad \text{as } \eta \to \infty$$

For $p_1 = 0$, $\frac{1}{2} K = E - \frac{1}{2} \beta^2 = 1.7346$.

$$\epsilon_1 = \frac{2}{u_e^2 \delta_1^2}$$

$$g_1'' + f_o g_1' - 2f_o' g_1 + 3\sigma \left(\frac{h_o - h_w}{H_e} \right) f_1 g_o'$$

$$= - \frac{p_1 \delta_1^2}{c u_e \rho_w} \frac{(h_o - h_w)}{H_e} \left(1 + \frac{h_o - h_w}{h_w} f_o' - \frac{u_e^2}{2h_w} f_o'^2 \right) \qquad (15a)$$

$$+ \omega \frac{[h_o \Omega - (h_o - h_w)\omega]}{H_e} (f_{\frac{1}{2}}' g_{\frac{1}{2}} - 2f_{\frac{1}{2}} g_{\frac{1}{2}}')$$

$$g_1(0) = 0$$

$$g_1(\eta) \to \frac{h_o \phi}{H_e}(\eta^2 - 2\beta\eta + \beta^2 + 1)$$

$$+ \frac{\omega K[h_o\Omega - (h_o - h_w)\omega]}{2H_e} + \frac{p_1 \delta_1^2}{c\rho_{ei}u_e}\frac{(h_o - h_w)}{2H_e}\left(\frac{h_o}{h_{ei}} - \frac{u_o^2}{2h_{ei}}\right) \text{ as } \eta \to \infty \qquad (15b)$$

In terms of these functions, one arrives at the following formulae, in which some anomalous expressions in reference 2 have been corrected.

$$u = u_e\left[f_o'(\eta) + \frac{(2s)^{\frac{1}{2}}}{u_e\delta_1}\omega f_{\frac{1}{2}}'(\eta) + \frac{2s}{u_e^2\delta_1^2}\left\{\omega^2 f_{\frac{1}{2}\frac{1}{2}}'(\eta) + \sigma f_1'(\eta)\right\} + O(s^{\frac{3}{2}})\right] \qquad (16)$$

$$H = h_w + (h_o - h_w)g_o(\eta) + \frac{(2s)^{\frac{1}{2}}}{u_e\delta_1}\left[(h_o - h_w)\omega f_{\frac{1}{2}}'(\eta)\right.$$

$$\left. + \left\{h_o\Omega - (h_o - h_w)\omega\right\}g_{\frac{1}{2}}(\eta)\right] + \frac{2s}{u_e^2\delta_1^2}\left\{(h_o - h_w)\omega^2 f_{\frac{1}{2}\frac{1}{2}}'(\eta) + H_e g_1(\eta)\right\} + O(s^{\frac{3}{2}}) \qquad (17)$$

Note that H_e is still undetermined. When p_1 is sufficiently small, one may expect the Crocco relation for the initial profiles, i.e., Eq. (6). This is the case for the profiles obtained by the inviscid and adiabatic expansion technique. Then $h_o\Omega - (h_o - h_w)\omega = 0$. Thus the last group of terms on the right-hand side of the differential equation in Eq. (15) disappears. Choose H_e such that

$$H_e = \sigma(h_o - h_w) \tag{18}$$

Then the differential equations, Eq. (15) for g_1 and Eq. (13) for f_1' become identical with identical boundary conditions provided $p_1 = 0$, because from Eqs. (6) and (18) one has

$$\frac{H_e}{h_o^{\bar{\Phi}}} = \frac{\sigma(h_o - h_w)}{h_o^{\bar{\Phi}}} = 1$$

Also, then it can be seen from Eqs. (16) and (17) that the Crocco relation exists for the inner profiles.

When p_1 is not small, the same relation cannot be expected for the outer and inner profiles. Then H_e may assume a value other than given by Eq. (18).

Tables of the functions $f_{\frac{1}{2}}$, $g_{\frac{1}{2}}$, . . . are given at the end of the report.*

The heat transfer rate at the wall can be expressed in a non-dimensional form as

$$\frac{Nu}{Re_s^{\frac{1}{2}}} = \frac{qC_{p_{se}}R_o}{\kappa_{se}(H_{ei} - h_w)} \frac{1}{Re_s^{\frac{1}{2}}} \tag{19}$$

where

$$q = \frac{\kappa}{C_p}\left(\frac{\partial H}{\partial \eta}\frac{\partial \eta}{\partial y}\right)_{y=0} = \frac{\kappa}{C_p \mu_w} \frac{u_o \rho_w \mu_w}{(2s)^{\frac{1}{2}}} \left(\frac{\partial H}{\partial \eta}\right)_{\eta=0}$$

where q is the amount of heat transferred per unit time area,

---

*The authors wish to thank Mr. T. Tani of the National Aeronautical Laboratory, Tokyo, Japan, for supplying them with the table of these functions.

$Re_s = \rho_{se}\sqrt{H_{ei}}\, R_o/\mu_{se}$ and the suffix se refers to the conditions after a normal shock of the undisturbed flow.

The experiments for a sharp cone-cylinder as well as for a blunt cone are described in reference 2. The pertinent flow quantities for the 20 degree sharp cone-cyliner are:

Stagnation pressure	= 600 psia
Stagnation temperature	= 1800°R
Wall-to-stagnation temperature ratio	= 0.313
Re_s	= 3×10^4
Free stream Mach number	= 8
Mach number outside the boundary layer	= 4.25 before the corner 6.63 after the corner

Using the experimental data q is obtained from Eq. (8). Then Eq. (19) finally results in

$$\frac{Nu}{Re_s^{\frac{1}{2}}} \cdot 10^3 = \frac{8.619}{\sqrt{x}} + 6.6 + 1.14\sqrt{x} + \cdots \qquad (20)$$

where p_1 is assumed zero and x is measured in inches. The results are plotted in Fig. 2. Also included for comparison is the flat plate solution corresponding to the uniform flow at the edge of the outer shear layer. The ratio of the fourth term in Eq. (20), which is omitted, to the third term is $O(\sqrt{x}/10)$ and is also proportional to $Re_s^{-\frac{1}{2}}$. For the present value of Re_s, the fourth term becomes of appreciable magnitude at x = 100 inches.

Also included is Van Driest's flat plate solution[5] in which assumptions (1) and (2) are relaxed. Correction to these effects can be easily made. However, as is evident from Fig. 2, present results show satisfactory agreement with the experiment for most engineering purposes.

In order to further substantiate the applicability of this theory, the results of the analysis are compared with the experimental results of reference 20.

The pertinent flow quantities for the 15° sharp cone-cylinder are:

Stagnation pressure	= 139 psia
Stagnation temperature	= 710°R
Wall-to-stagnation temperature ratio	- refer to Fig. 3
Re_s	= 3.74×10^5
Free stream Mach number	= 5
Mach number outside the boundary layer	= 3.8 before the corner 5.12 after the corner

From these data, Eq. (19) finally results in

$$\frac{Nu}{Re_s^{\frac{1}{2}}} \cdot 10^3 = \frac{2.3295}{\sqrt{x}} + 1.693 + \cdots \qquad (20a)$$

where p_1 is assumed zero and x is measured in inches, and the initial profiles are lincarized. The results are plotted in Fig. 3. Again, the results show satisfactory agreement with the experiment. The experimental data have been replotted in terms of the Nusselt number and

Reynolds number defined in this paper.

Finally, consideration is given to the applicability of the sublayer model. The concept of the sublayer model is entirely dependent on the characteristics of the initial velocity profile at the corner which, after being expanded abruptly, has a slipping portion on the wall right at the corner. Hence, the corner becomes a singular point at which the sublayer may be assumed to start.

If, on the other hand, this slipping portion is missing in the initial profile the sublayer cannot be expected to start even if other flow quantities may change discontinuously at that point. Such an example may be given of the flow field immediately downstream of a localized injection over a flat plate. It can be shown that even if one starts with the sublayer model, one finally arrives at a merged layer of Couette type flow which indicates that the sublayer does not start at the end of the injection region.

SECTION III
TURBULENT FLOW

For turbulent flows, mathematical treatment becomes increasingly difficult. Nevertheless, it will be shown here that the sublayer model coupled with some simple physical arguments results in a sufficiently accurate prediction of the heat transfer rate. For this case the boundary layer ahead of the corner will be turbulent. Two cases will be considered here. The first case will be for the condition

where the boundary layer is artificially tripped, and the second case will be for the condition where the free stream Reynolds number is sufficiently high for a turbulent boundary layer to be established before the corner.

A. Method of Analyzing Boundary Layer Upstream of the Corner

In order to insure that the boundary layer ahead of the corner was turbulent, the heat transfer rate in each case was calculated using standard turbulent boundary layer analysis. The velocity and enthalpy profiles ahead of the corner were calculated by using the tabulations of reference 7 for a (1/7)th power law for the velocity profile.

In what follows, a formula for the heat transfer rate on a cone, Eqs. (26) and (30) and that for a flat plate, Eqs. (26) through (28) are derived. These formulae will be used for the conical part of the body and for the cylindrical afterbody respectively. The main procedure is such that the flow field is transformed by the Howarth transformation into a constant density reference state which may be regarded as incompressible flow field so that the empirical power law profile for a flat plate may be applied. Also, the reference enthalpy method is naturally arrived at. For a cone, Van Driest's law is applicable to convert the flat plate skin friction values.

The boundary layer equations for a turbulent flow over a flat plate are given by

$$\left.\begin{aligned} &\frac{\partial}{\partial x}(\overline{\rho u}) + \frac{\partial}{\partial y}(\overline{\rho v}) = 0 \\ &\overline{\rho}\,\overline{u}\frac{\partial \overline{u}}{\partial x} + \overline{\rho v}\frac{\partial \overline{u}}{\partial y} = \frac{\partial}{\partial y}\left[\overline{\mu}\frac{\partial \overline{u}}{\partial y} - \overline{\rho}\,\overline{u'v'}\right] \\ &\overline{\rho}\,\overline{u}\frac{\partial \overline{H}}{\partial x} + \overline{\rho v}\frac{\partial \overline{H}}{\partial y} = \frac{\partial}{\partial y}\left[\overline{\mu}\frac{\partial \overline{H}}{\partial y} - \overline{\rho}\,\overline{H'v'}\right] \end{aligned}\right\} \qquad (21)$$

where bar implies time average. Also it is assumed that $\frac{\partial \overline{p}}{\partial x} = 0$ and $Pr_L = \frac{\overline{C}_p \overline{\mu}}{\overline{\kappa}} = 1$. Introduce the stream function such that

$$\overline{\rho}\,\overline{u} = \rho_* \frac{\partial \psi}{\partial y} \quad , \quad \overline{\rho v} = -\rho_* \frac{\partial \psi}{\partial x}$$

where star denotes the unspecified reference conditions. Then the Howarth transformation

$$x_* = x \quad , \quad y_* = \int_0^y \frac{\overline{\rho}}{\rho_*}\, dy$$

is applied. Following Mager[8], the following quantities are assumed invariant.

(1) the stream function $\psi = \psi_*$ where

$$u_* = \frac{\partial \psi_*}{\partial y_*} \quad , \quad v_* = -\frac{\partial \psi_*}{\partial x_*}$$

(2) the turbulent shear per elemental mass

$$\overline{\rho}\,(\overline{u'v'}) = \rho_*(\overline{u'v'})_*$$

(3) $\overline{\rho}\,\overline{\mu} = \rho_*\mu_*$

Eqs. (21) become

$$\left.\begin{aligned} u_* \frac{\partial u_*}{\partial x_*} + v_* \frac{\partial u_*}{\partial y_*} &= \frac{\partial}{\partial y_*}\left[\nu_* \frac{\partial u_*}{\partial y_*} - (\overline{u'v'})_*\right] \\ u_* \frac{\partial \bar{H}}{\partial x_*} + v_* \frac{\partial \bar{H}}{\partial y_*} &= \frac{\partial}{\partial y_*}\left[\nu_* \frac{\partial \bar{H}}{\partial y_*} - \frac{\partial \bar{H}/\partial y_*}{\partial \bar{u}_*/\partial y_*} (\overline{u'v'})_*\right] \end{aligned}\right\} \quad (22)$$

where use has been made of unity of the turbulent Prandtl number

$$Pr_T = \frac{\bar{\rho}\,\overline{u'v'}}{\bar{\rho}\,\overline{h'v'}} \frac{\partial \bar{h}/\partial y}{\partial \bar{u}/\partial y} .$$

Upon comparing these equations, the Crocco relation is obtained.

$$\bar{H} = h_w + \frac{H_e - h_w}{u_e} u_* \quad (23)$$

From which the Reynolds analogy results directly.

$$St = \frac{q}{\rho_e u_e (H_e - h_w)} = \frac{\rho_*}{\rho_e} \frac{c_{f_*}}{2} \quad (24)$$

where $c_{f_*}/2 = \mu_* \left.\frac{\partial u_*}{\partial y_*}\right|_{y_*=0} / \rho_* u_e^2$.

If the empirical correction is made to Prandtl number being other than unity, then

$$St = Pr_{av}^{-\frac{2}{3}} \frac{\rho_*}{\rho_e} \frac{c_{f_*}}{2} \tag{24'}$$

The Blasius skin friction formula for $(1/n)_{th}$ power profile gives

$$\frac{c_{f_*}}{2} = \frac{1}{\left\{c(n)\right\}^{\frac{2n}{n+3}}} \left\{\frac{n}{(n+2)(n+3)}\right\}^{\frac{2}{n+3}} Re_x^{*\,-\frac{2}{n+3}} \tag{25}$$

where $Re_x^* = \frac{U_e x}{\nu_*}$ and c(n) is given in reference 9. Combining Eqs. (25) and (24), the following expression for the Nusselt number is obtained.

$$Nu = St \cdot Re_x \cdot Pr_{av} = Pr_{av}^{\frac{1}{3}} \cdot \frac{c_f}{2} \cdot Re_x \tag{26}$$

where

$$\frac{1}{2} c_f = \frac{(\bar{\mu} \frac{\partial \bar{u}}{\partial y})_{y=0}}{\rho_e u_e^2}$$

$$= \frac{1}{\left\{c(n)\right\}^{\frac{2n}{n+3}}} \left\{\frac{n}{(n+2)(n+3)}\right\}^{\frac{2}{n+3}} \left(\frac{\mu_e}{\rho_e u_e x}\right)^{\frac{2}{n+3}} \left(\frac{\mu_*}{\mu_e}\right)^{\frac{2}{n+3}} \left(\frac{\rho_*}{\rho_e}\right)^{1-\frac{2}{n+3}} \tag{27}^*$$

*See footnote on page 17..

*Footnote for page 16.

After completion of the manuscript, the authors' attention has been called to a skin friction formula given by Spence[10].

$$\frac{1}{2} c_f = \frac{\rho_*}{\rho_e} \left\{c(n)\right\}^{-\frac{2n}{n+1}} \left(\frac{\rho_e}{\rho_*} \frac{u_e \Delta}{\nu_*}\right)^{-\frac{2}{n+1}}$$

where

$$\frac{u}{u_e} = \left(\frac{\eta}{\Delta}\right)^{\frac{1}{n}}$$

$$\eta = \int_o^y \frac{\rho}{\rho_e} \, dy$$

$$\Delta = \int_o^{edge} \frac{\rho}{\rho_e} \, dy$$

It can be shown that this formula is exactly identical with Eq. (27). In the reference state, the thickness of the boundary layer is given by

$$\delta = \int_o^{edge} \frac{\rho}{\rho_*} \, dy = \frac{\rho_e}{\rho_*} \Delta$$

$$= \frac{1}{\left\{c(n)\right\}^{\frac{2n}{n+3}}} \left\{\frac{(n+2)(n+3)}{n}\right\}^{\frac{n+1}{n+3}} \left(\frac{\nu_*}{u_e x}\right)^{\frac{2}{n+3}} x$$

Eq. (27) is arrived at if the above expression is inserted into the foregoing formula.

(End of footnote.)

Since

$$\frac{1}{2}\,(c_f)_{\substack{\text{incomp.}\\ \text{flat plate}}} = \frac{1}{\left\{c(n)\right\}^{\frac{2n}{n+3}}} \left\{\frac{n}{(n+2)(n+3)}\right\}^{\frac{2}{n+3}} \left(\frac{\mu_e}{\rho_e u_e x}\right)^{\frac{2}{n+3}} \tag{28}$$

is one-half of the skin-friction coefficient of an incompressible flow with the flow quantities corresponding to the outer edge conditions, the factor

$$\left(\frac{\mu_*}{\mu_e}\right)^{\frac{2}{n+3}} \left(\frac{\rho_*}{\rho_e}\right)^{1-\frac{2}{n+3}}$$

is the one connecting the compressible skin friction coefficient to the incompressible reference state. For $n=7$, $(\mu_*/\mu_e)^{0.2}(\rho_*/\rho_e)^{0.8}$ is the factor usually used in the reference enthalpy method[11]. Accordingly, the undetermined reference state is taken as given by

$$h_* = 0.5(h_w+h_e) + 0.22(h_{aw}-h_e) \tag{29}$$

with $h_{aw}=h_e + Pr_{av}^{\frac{1}{3}} \frac{u_e^2}{2}$. Further support for this step may be found in the work of Burggraf[12] who proceeded to substantiate the method. He proposes the reference state as that of the outer edge of the laminar sublayer which was first suggested by Rott[13].

For a not so-slender cone in a supersonic flow with attached bow shock wave, Van Driest's law[14] may be applied to calculate the skin friction and hence the heat transfer. According to this rule, the cone

skin friction is evaluated with one-half the Reynolds number for flat plate with the same free stream Mach number and the same wall-to-free-stream temperature ratio. Thus, from Eqs. (27) and (28) one gets

$$\frac{1}{2} c_{f_{cone}} = 2^{\frac{2}{n+3}} \left(\frac{\mu_*}{\mu_e}\right)^{\frac{2}{n+3}} \left(\frac{\rho_*}{\rho_e}\right)^{1-\frac{2}{n+3}} \frac{1}{2} (c_f)_{\substack{\text{incomp.} \\ \text{flat plate}}} \tag{30}$$

The correction factor in this expression can be written in terms of the Mach number and the wall-to-free-stream temperature ratio. For example, assuming $n = 7$ and

$$\frac{\mu_*}{\mu_e} = \left(\frac{T_*}{T_e}\right)^{0.75}$$

one obtains

$$2^{0.2} \left(\frac{\mu_*}{\mu_e}\right)^{0.2} \left(\frac{\rho_*}{\rho_e}\right)^{0.8} = 1.15 \left\{0.5\left(1 + \frac{T_w}{T_e}\right) + 0.22 \frac{\gamma-1}{2} M_e^2\right\}^{-\frac{1}{2}} .$$

B. Expansion Around the Corner

In this step the viscosity is neglected. The velocity and stagnation enthalpy profiles are expanded isentropically around the corner. In this manner a velocity profile having a non-zero value at the wall and a corresponding stretched-out stagnation enthalpy profile is obtained downstream of the corner. This scheme has been proposed in reference 1, and has been used successfully in reference 2. Reference 1 points out that the high acceleration present at the corner

has an effect of reducing the turbulence level in the boundary layer. This is similar to the reduction in turbulence level obtained by the contraction section of a wind tunnel. Morkovin[15] has made a detailed study of the effect of a sudden expansion on a turbulent boundary layer. In this study, the expansion was produced on a flat plate by means of a wedge. Detailed profile measurements of pitot pressure and velocity fluctuations before and after the expansion were made. The results indicated that the assumption of isentropy in the boundary layer during the expansion is valid. The measurements of the velocity fluctuations in percent of local mean velocity before and after the corner indicated a decrease close to the wall, and an increase towards the outside part of the boundary layer. Therefore, the results of references 1, 2, and 15 justify the inviscid expansion assumed in this part of the paper. In each case the momentum thickness after the expansion is calculated from the density and velocity profiles obtained after the expansion with the following equation:

$$\theta = \int_0^{\delta} \frac{\rho u}{\rho_e U_e} \left(1 - \frac{u}{U_e}\right) d\eta \qquad (31)$$

C. Analysis of Boundary Layer Downstream of Corner

Reference 1 has indicated that the effect of a large pressure expansion around the corner enables the growth of a new laminar boundary layer starting at the beginning of the cylinders. It is also believed[1] that the extent of the new laminar boundary layer, and the transition to turbulent flow, is controlled by the high turbulence level present in the

shear layers after the expansion.

The concept given above is a result of dealing with the micro-scale turbulence level present in the boundary layer before and after the corner. These results have not been confirmed substantially and are not amenable to be used in calculating the heat transfer. Therefore, in this paper in a manner analogous to that of determining transition over a flate plate, the momentum thickness will be used as a measure of the transition to turbulence.

Therefore, it is important for this case to calculate the Reynolds number based on the momentum thickness before and after the corner. It will also be demonstrated in a subsequent section that Re_θ is indicative of the extent of the laminar sublayer after the corner.

Therefore, since the initial part of the boundary sublayer after the corner is laminar, analysis developed for the laminar sublayer is also applicable here. The shear profiles for the laminar sublayer will be the ones obtained from the inviscid expansion of the turbulent profiles obtained ahead of the corner. In this it is assumed that the fluctuations in the shear layer have a negligible effect on the formulation of the laminar sublayer.

Next, consideration will be given to the development of the asymptotic flow downstream of the corner. It is well-known that turbulent boundary layer profiles at high Reynolds number preserve their self-similar character over the greater part of the flow provided there is no pressure gradient[16,17]. For the present case, despite the negligibly small pressure gradient, self-similarity may not be expected

within at least some distance downstream of the corner. This is due to the transient state immediately after the rapid expansion. The flow must adjust itself for some distance until it approaches the asymptotic state where the self-similar character prevails again. This state may be reached roughly when the sublayer swallows up the mass flow contained in the initial velocity profile immediately after the corner. Thus, the complicated transient phenomenon of the overall viscous layer is now replaced by the changing proportion of the sublayer and the shear layer; the latter is absorbed in the former. In this argument a simplifying assumption has been made that the velocity profile of the outer shear layer does not change appreciably for the range considered. In other words, additional mass entrained within the shear layer and the displacement effect of the sublayer on the shear layer are neglected. Further simplifications may be made by approximating linearly the average initial profiles immediately after the corner. The sublayer will be first assumed fully turbulent from the corner. Since it is assumed to preserve its self-similar character all the way, (1/7)th power law is adopted for the velocity profile. Correspondingly, the heat transfer rate can be calculated with the flat plate equations. The proper outer edge conditions correspond to those of the initial profiles obtained right after expansion. These outer edge conditions will provide the asymptotic solution. Having now established the turbulent asymptotic solution to the problem at some distance away from the corner, and also having established the laminar region immediately downstream of the corner, it is now necessary to connect the two

solutions. In this, a study of transition is necessary in order to obtain the complete solution.

The transitional region is analyzed following references 18 and 19. Use is made of the same simplifying assumption that the profiles of the outer shear layer do not change appreciably for the range considered. The growth of the sublayer in the transformed plane is determined by solving the momentum equation using the empirical skin friction expression in terms of $Re_{\theta_*} = \frac{\nu_{e_*}}{U_{e_*}\theta_*}$.

$$\frac{d\theta_*}{dx} = \frac{c_{f_*}}{2} \tag{32}$$

$$c_{f_*} = \mu_* \frac{\partial u_*}{\partial y_*}\Big|_{y_*=0} \Big/ \frac{\rho_* u_e^2}{2} = 0.0261\, Re_{\theta_*}^{-\frac{1}{4}} - D\, Re_{\theta_*}^{-2} \tag{33}$$

Correspondingly, the thickness of the transitional sublayer is determined by the following relation:

$$\left(\frac{\delta_*}{\theta_*}\right)_{trans} = \left(\frac{\delta_*}{\theta_*}\right)_{turb} - \frac{G}{x}\left(\frac{\delta_*}{\theta_*}\right)_{lam} \tag{34}$$

where the constants D and G are obtained by matching c_{f_*} and $(\frac{\delta_*}{\theta_*})_{trans}$ with those of the laminar flow at the assumed transition point. Eq. (32) is integrated numerically, yielding the distribution of the momentum thickness. From the local thickness of the sublayer and from the

initial profiles of the outer shear layer, the local outer edge conditions of the sublayer are determined. From Eq. (33) the local skin friction and hence the local heat transfer rate are obtained.

SECTION IV

DISCUSSION OF THEORETICAL AND EXPERIMENTAL RESULTS

In order to demonstrate the various theoretical aspects discussed in the previous section, four experimental results are presented below.

Case 1.

Stagnation pressure	= 600 psia
Stagnation temperature	= 1700°R
Wall-to-stagnation temperature ratio	= 0.294
$Re_s = \frac{\rho_{se}\sqrt{H_{ei}}\, R_o}{\mu_{se}}$ ($R = 0.582''$)	$= 4.94 \times 10^4$
Free stream Mach number	= 8
Mach number outside the boundary layer	= 1.70 before the corner 2.67 after the corner

The above test was conducted at the hypersonic facility of the Polytechnic Institute of Brooklyn. The body consists of a spherically capped 24° half angle cone-cylinder, with a bluntness ratio of $R_o/r = 0.317$ (Fig. 4). The laminar boundary layer study over this body has been presented in reference 2. Experimental laminar heat transfer results, as well as comparison with theory before and after

the corner, were also included in reference 2. In order to make the boundary layer turbulent ahead of the corner, trips were placed at the nose portion of the model in order to induce transition. The pressure distribution over the model was measured with the trips and indicated that there was no change from the one obtained without the trips. Therefore, in these analyses the pressure distribution presented in reference 2 was used in calculating the heat transfer before and after the corner. The heat transfer measurements are presented in Fig. 4 in the form of $Nu/\sqrt{Re_s}$ versus x in inches. In order to insure that the boundary layer before the corner was turbulent, standard heat transfer analysis was used to predict the heat transfer before the corner. The boundary layer profiles ahead of the corner have been calculated with the technique described in Section III and are presented in Fig. 4a. The Reynolds number based on the momentum thickness calculated for the profiles is $Re_\theta = 208$. The profiles obtained after the inviscid expansion around the corner are presented in Figure 4b. The expansion in this case has a two-fold effect on Re_θ. First it tends to increase the momentum thickness after the expansion, and secondly it reduces the density due to the expansion. The Reynolds number based on the momentum thickness after the expansion is 143. This is sufficiently low to enable a new laminar boundary layer to prevail for quite a large distance after the corner. The heat transfer after the corner was therefore calculated with the aid of the laminar boundary layer Eqs. (17) and (19) using the turbulent shear profiles presented in Fig. 4b. The results are presented in Fig. 4, and it is clearly seen that the experimental

data is well represented by the theory presented here. On the same figure, the turbulent solution for the heat transfer for the asymptotic state is also presented for verifying that the boundary layer obtained after the expansion is laminar. It is expected that this new laminar boundary layer will prevail for quite a distance downstream of the corner since the Reynolds number based on the momentum thickness is low.

Case 2. (Reference 6)

Stagnation pressure	= 57.3 psia
Stagnation temperature	= 660°R
Wall-to-stagnation temperature ratio	= 0.924
Re_s	= 5.13×10^6
Free stream Mach number	= 3.04
Mach number outside the the boundary layer	= 1.88 before the corner 2.39 after the corner

The results of these tests have been taken from reference 6. The body tested consisted of a spherically capped 15° half angle cone with a bluntness ratio of $R_o/r = 0.6$ (Fig. 6).

For the test conditions presented above, the Reynolds number was sufficiently high so that a turbulent boundary layer was well established ahead of the corner. In order to substantiate this, the turbulent heat transfer has been calculated ahead of the corner, and is presented in Fig. 6 with the measurements. It is clearly seen that the experimental results are well presented by the turbulent solution. Fig. 5a presents the boundary layer profiles before the corner. In this

case, Re_θ was calculated to be 750. The shear layer profiles obtained after the inviscid expansion around the corner are presented in Fig. 5b. For this condition Re_θ was calculated to be 770. Therefore, in this case, the expansion around the corner was not sufficient to make up for the increase in the momentum thickness, and therefore for this condition it would be expected that the second transition to turbulent flow would occur in a rather short distance after the corner.

Since a laminar boundary layer does prevail after the discontinuity, the heat transfer has been calculated according to reference 2 and is presented in Fig. 6. On the same figure, the asymptotic solution of the turbulent boundary layer is also presented. It is clearly indicated that transition occurs between $x = 0.5 \rightarrow 1.0$ inches. In this case transition was chosen to occur at an $Re_\theta \approx 1100$ (approximate flat plate value) corresponding to $x = 0.75$ inches. With this, the transitional heat transfer was calculated with the aid of Eq. (32) and (33), and is included in Fig. 6.

The previous experiment, and the considerations presented in this paper bear out well that a laminar sublayer is followed by a second transition to turbulent flow.

Case 3

Stagnation pressure	= 139 psia
Stagnation temperature	= 710°R
Wall-to-stagnation temperature ratio	= 0.47
Re_s	= 3.73×10^5
Free stream Mach number	= 5.0
Mach number outside the boundary layer	= 3.8 before the corner 5.12 after the corner

The results of these tests have been taken from reference 20. The body consisted of a 15° half angle sharp cone followed by a cylindrical afterbody 1.8" in diameter. The laminar results for this configuration have been presented in the Laminar portion of this paper. In order to obtain a turbulent boundary layer, trips were placed on the conical portion of the body. The results of the heat transfer measurements are presented in Fig. 7 in terms of the symbols used in this report. The Reynolds number based on the turbulent momentum thickness ahead of the corner was calculated to be 1370, while the one calculated after the expansion was 1530. The analysis for the laminar calculations as well as for the turbulent asymptotic solution are included in Fig. 7. For this case the Re_θ after the corner is sufficiently large so that the laminar sublayer is swallowed in a very short distance after the corner. Therefore, the boundary layer is closely approximated by the asymptotic turbulent solution. These considerations are clearly seen from the theoretical predictions included in

Fig. 7. The experimental results are much higher than the laminar predictions, and are closer to the turbulent asymptotic solution.

Case 4.

In order to further substantiate the fact that the extend of the laminar sublayer after the corner may be obtained from Re_θ, the experimental results of reference 1 are used.

Stagnation pressure	= 27.1 psia
Stagnation temperature	= 535°R
Wall-to-stagnation temperature ratio	= adiabatic wall
Re_s	= 5.352×10^6
Free stream Mach number	= 3.02
Mach number outside the boundary layer	= 1.89 before the corner 3.13 after the corner

The body considered in the above test consisted of a 29° half angle sharp cone. The adiabatic wall temperature was measured before and after the corner for both laminar as well as turbulent conditions ahead of the corner. For the case where a laminar region prevailed ahead of the corner, Re_θ is calculated to be 540. Inviscid profiles after the corner were also obtained, and the corresponding Re_θ calculated for these profiles was 460. It is indicated in reference 1 that transition for this case was observed to occur at a distance of 20 centimeters downstream of the shoulder. Since for this condition the heat transfer is zero, the momentum thickness is calculated from the skin friction coefficient, which is in turn calculated from the theoretical predictions

given in the Laminar section of the paper. A value of Re_θ equal to 1200 was obtained from the analysis at the observed station of transition.

For the case where the boundary layer was turbulent ahead of the corner, the value of Re_θ calculated before and after the corner is 1200 and 800 respectively. The portion where transition was observed for this condition was at 3 centimeters downstream of the shoulder, the Re_θ calculated at the point of transition was equal to 1100. Therefore, for this condition the boundary layer is predominantly turbulent as indicated in the Turbulent Flow section of this paper. What is more important is the fact that transition occurred approximately at the same value of Re_θ as for the laminar case. Therefore, the assumption of neglecting the fluctuations in the shear layer in analyzing the boundary layer and the criterion that Re_θ is indicative of transition in this case, has clearly been demonstrated.

SECTION V

CONCLUSIONS

A flow model has been adopted for treating the boundary layer downstream of a sharp corner. The analysis based on this model for a laminar flow was presented in reference 2. Improvements are made herein whereby a unified treatment of velocity and thermal profiles based on the Crocco relation holds, thus are amenable to the calculation of the higher order solutions including the pressure gradient as perturbation.

An extension of this flow model to conditions where the boundary layer ahead of the corner is turbulent, is also included. These results were compared with some of the experimental results available in the literature.

The results also reaffirmed the considerations presented by Sternberg that a new laminar boundary layer does start at the discontinuity. This boundary layer will prevail for a distance, and a second transition to turbulent will subsequently occur.

It is indicated here that for the range of test conditions observed, that if Re_θ before the discontinuity is of the order of 600 → 700, then a turbulent boundary layer exists ahead of the discontinuity. The expansion around the corner has a two-fold effect on Re_θ. The first is an increase in the momentum thickness θ, and a decrease in the density. Based on the calculation of Re_θ after the corner, an idea where transition occurs on the cylinder may be obtained. It is indicated from the results presented here that the second transition to turbulent occurred at an Re_θ of the order of 1100 → 1500. For the case where Re_θ is larger than 1400 after the expansion, the heat transfer is predominantly turbulent and may be estimated from the asymptotic turbulent analysis. Based on these considerations, calculations for the full laminar, transitional, and turbulent boundary layer after the discontinuity are then presented. It is also indicated here that the effect of shear on the development of the turbulent boundary layer after the discontinuity is of much less significance than for the laminar case.

SECTION VI

REFERENCES

1. Sternberg, J.: The Transition from a Turbulent to a Laminar Boundary Layer. BRL Report No. 906, May 1954.
2. Zakkay, V. and Tani, T.: Theoretical and Experimental Investigation of the Laminar Heat Transfer Downstream of a Sharp Corner. Polytechnic Institute of Brooklyn, PIBAL Report No. 708, AFOSR 1640, October 1961; also Proceedings of the Fourth U. S. National Congress of Applied Mechanics, Vol. 2, pp. 1455-1467, American Society of Mechanical Engineering, New York, 1962.
3. Li, T. Y.: Effects of Free-Stream Vorticity on the Behavior of a Viscous Boundary Layer. J. Aero. Sci., 23, 12, pp. 1128-1129, December 1956.
4. Glauert, M. B.: The Boundary Layer in Simple Shear Flow Past a Flat Plate. J. Aero. Sci., 24, 11, pp. 848-849, November 1957.
5. Van Driest, E. R.: The Turbulent Boundary Layer with Variable Prandtl Number. Chapter in Fifty Years of Boundary Layer Theory, Braunschweig, Germany: Viewig, 1955.
6. Inouye, M. and Sisk, J. B.: Wind-Tunnel Measurements at Mach Numbers from 3 to 5 of Pressure and Turbulent Heat Transfer on a Blunt Cone-Cylinder with Flared Afterbody. (Title Unclassified). NASA TM X-654, July 1962. CONFIDENTIAL. (Figs. 4 and 7 were declassified February 12, 1963.)

7. Persh, J. and Lee, R.: Tabulation of Compressible Turbulent Boundary Layer Parameters. NAVORD Report No. 4282, 1956.

8. Mager A.: Transformation of the Compressible Turbulent Boundary Layer. J. Aero. Sci., 25, 5, pp. 305-311, May 1958.

9. Schlichting, H.: Boundary Layer Theory. McGraw-Hill Book Co., Inc., New York, 4th ed., p. 507, 1960.

10. Spence, D. A.: Distributions of Velocity, Enthalpy and Shear Stress in the Compressible Turbulent Boundary Layer on a Flat Plate. RAE Report No. AERO. 2631, November 1959.

11. Eckert, E. R. G.: Engineering Relations for Friction and Heat Transfer to Surfaces in High Velocity Flow. J. Aero. Sci., 22, 8, pp. 585-587, August 1955.

12. Burggraf, O. R.: The Compressibility Transformation and Turbulent Boundary Layer Equations. J. Aero. Sci., 29, 4, pp. 434-439, April 1962.

13. Rott, N.: On the Transfer of Heat and Mass in the Turbulent Boundary Layer. Ramo-Wooldridge Corp. Report No. GM-TR-211, 1957.

14. Van Driest, E. R.: Turbulent Boundary Layer on a Cone in a Supersonic Flow at Zero Angle of Attack. J. Aero. Sci., 19, 1, pp. 55-57, January 1952.

15. Morkovin, M. V.: Effects of High Acceleration on a Turbulent Supersonic Shear Layer. Heat Transfer and Fluid Mechanics Institute, Los Angeles, California, 1955.

16. Lin, C. C. (Editor): Turbulent Flows and Heat Transfer. Princeton Series on High Speed Aerodynamics and Jet Propulsion. Vol. V, Princeton University Press, New Jersey, 1959.

17. Townsend, A. A.: The Structure of Turbulent Shear Flow. Cambridge University Press, New York, 1956.

18. Persh, J.: A Procedure for Calculating the Boundary-Layer Development in the Region of Transition from Laminar to Turbulent Flow. NAVORD Report No. 4438, 1957.

19. Zakkay, V. and Callahan, C. J.: Laminar, Transitional, and Turbulent Heat Transfer to a Cone-Cylinder-Flare Body at Mach 8.0. Polytechnic Institute of Brooklyn, PIBAL Report No. 737, AFOSR 2359, AD 274 122, February 1962; also J. Aero. Sci., 29, 12, pp. 1403-1420, December 1962.

20. Schaefer, J. W. and Ferguson, H.: Investigation of Separation and the Associated Heat Transfer and Pressure Distribution on Cone-Cylinder-Flare Configurations at Mach 5. Paper presented at American Rocket Society Space Flight Report to the Nation, New York, October 9-15, 1961.

TABLE 1

η	$f_{\frac{1}{2}}$	$f_{\frac{1}{2}}'$	$f_{\frac{1}{2}}''$
0	0	0	0.7950
0.2	0.0159	0.1590	0.7945
0.4	0.0636	0.3176	0.7910
0.6	0.1429	0.4750	0.7818
0.8	0.2534	0.6298	0.7646
1.0	0.3945	0.7802	0.7381
1.2	0.5651	0.9244	0.7029
1.4	0.7638	1.0610	0.6615
1.6	0.9889	1.1890	0.6185
1.8	1.2388	1.3087	0.5799
2.0	1.5119	1.4216	0.5521
2.2	1.8072	1.5306	0.5407
2.4	2.1241	1.6392	0.5486
2.6	2.4631	1.7513	0.5760
2.8	2.8252	1.8707	0.6197
3.0	3.2120	2.0000	0.6746
3.2	3.6259	2.1418	0.7344
3.4	4.0692	2.2937	0.7931
3.6	4.5441	2.4577	0.8462
3.8	5.0529	2.6315	0.8908
4.0	5.5973	2.8134	0.9260
4.2	6.1787	3.0014	0.9521
4.4	6.7982	3.1937	0.9703
4.6	7.4564	3.3891	0.9825
4.8	8.1539	3.5864	0.9901
5.0	8.8911	3.7849	0.9946
5.2	9.6680	3.9841	0.9972
5.4	10.4847	4.1838	0.9987
5.6	11.3415	4.3836	0.9994
5.8	12.2382	4.5835	0.9997
6.0	13.1749	4.7834	0.9999

TABLE 2

η	$g_{\frac{1}{2}}$	$g_{\frac{1}{2}}'$
0	0	0.4572
0.2	0.0915	0.4575
0.4	0.1831	0.4595
0.6	0.2755	0.4649
0.8	0.3694	0.4752
1.0	0.4660	0.4918
1.2	0.5666	0.5154
1.4	0.6726	0.5465
1.6	0.7856	0.5846
1.8	0.9069	0.6286
2.0	1.0374	0.6767
2.2	1.1777	0.7267
2.4	1.3280	0.7760
2.6	1.4879	0.8223
2.8	1.6566	0.8639
3.0	1.8331	0.8994
3.2	2.0159	0.9284
3.4	2.2040	0.9509
3.6	2.3959	0.9676
3.8	2.5907	0.9795
4.0	2.7874	0.9875
4.2	2.9855	0.9927
4.4	3.1844	0.9959
4.6	3.3838	0.9978
4.8	3.5834	0.9988
5.0	3.7833	0.9994
5.2	3.9832	0.9997
5.4	4.1831	0.9998
5.6	4.3831	0.9999
5.8	4.5831	0.9999
6.0	4.7831	1.0000

TABLE 3

η	f_1	f_1'	f_1''
0	0	0	1.1564
0.2	0.0232	0.2312	1.1564
0.4	0.0926	0.4626	1.1564
0.6	0.2082	0.6938	1.1568
0.8	0.3700	0.9254	1.1582
1.0	0.5784	1.1574	1.1634
1.2	0.8332	1.3912	1.1768
1.4	1.1350	1.6292	1.2056
1.6	1.4854	1.8752	1.2598
1.8	1.8860	2.1354	1.3506
2.0	2.3410	2.4186	1.4898
2.2	2.8558	2.7352	1.6866
2.4	3.4382	3.0974	1.9464
2.6	4.0986	3.5180	2.2682
2.8	4.8500	4.0086	2.6462
3.0	5.7074	4.5794	3.0692
3.2	6.6876	5.2382	3.5234
3.4	7.8090	5.9900	3.9952
3.6	9.0900	6.8368	4.4722
3.8	10.5500	7.7786	4.9448
4.0	12.2076	8.8140	5.4076
4.2	14.0816	9.9408	5.8576
4.4	16.1898	11.1562	6.2952
4.6	18.5498	12.4580	6.7214
4.8	21.1786	13.8442	7.1390
5.0	24.0930	15.3132	7.5500
5.2	27.3094	16.8640	7.9566
5.4	30.8440	18.4956	8.3602
5.6	34.7130	20.2080	8.7622
5.8	38.9326	22.0004	9.1630
6.0	43.5186	23.8732	9.5636

TABLE 4 ($f_{\frac{1}{2}\frac{1}{2}}$ for $p_1 = 0$)

η	$f_{\frac{1}{2}\frac{1}{2}}$	$f_{\frac{1}{2}\frac{1}{2}}'$	$f_{\frac{1}{2}\frac{1}{2}}''$
0	0	0	0.1576
0.2	0.0031	0.0316	0.1576
0.4	0.0126	0.0630	0.1576
0.6	0.0283	0.0946	0.1578
0.8	0.0505	0.1262	0.1591
1.0	0.0788	0.1584	0.1631
1.2	0.1138	0.1919	0.1730
1.4	0.1559	0.2282	0.1933
1.6	0.2055	0.2701	0.2287
1.8	0.2645	0.3210	0.2829
2.0	0.3348	0.3846	0.3560
2.2	0.4194	0.4644	0.4434
2.4	0.5217	0.5623	0.5350
2.6	0.6455	0.6778	0.6179
2.8	0.7939	0.8078	0.6780
3.0	0.9692	0.9468	0.7047
3.2	1.1727	1.0872	0.6932
3.4	1.4036	1.2216	0.6452
3.6	1.6604	1.3433	0.5687
3.8	1.9398	1.4479	0.4752
4.0	2.2383	1.5331	0.3766
4.2	2.5518	1.5989	0.2836
4.4	2.8767	1.6474	0.2030
4.6	3.2098	1.6812	0.1383
4.8	3.5485	1.7038	0.0898
5.0	3.8908	1.7181	0.0557
5.2	4.2353	1.7267	0.0331
5.4	4.5813	1.7319	0.0191
5.6	4.9279	1.7348	0.0107
5.8	5.2750	1.7365	0.0061
6.0	5.6224	1.7374	0.0036

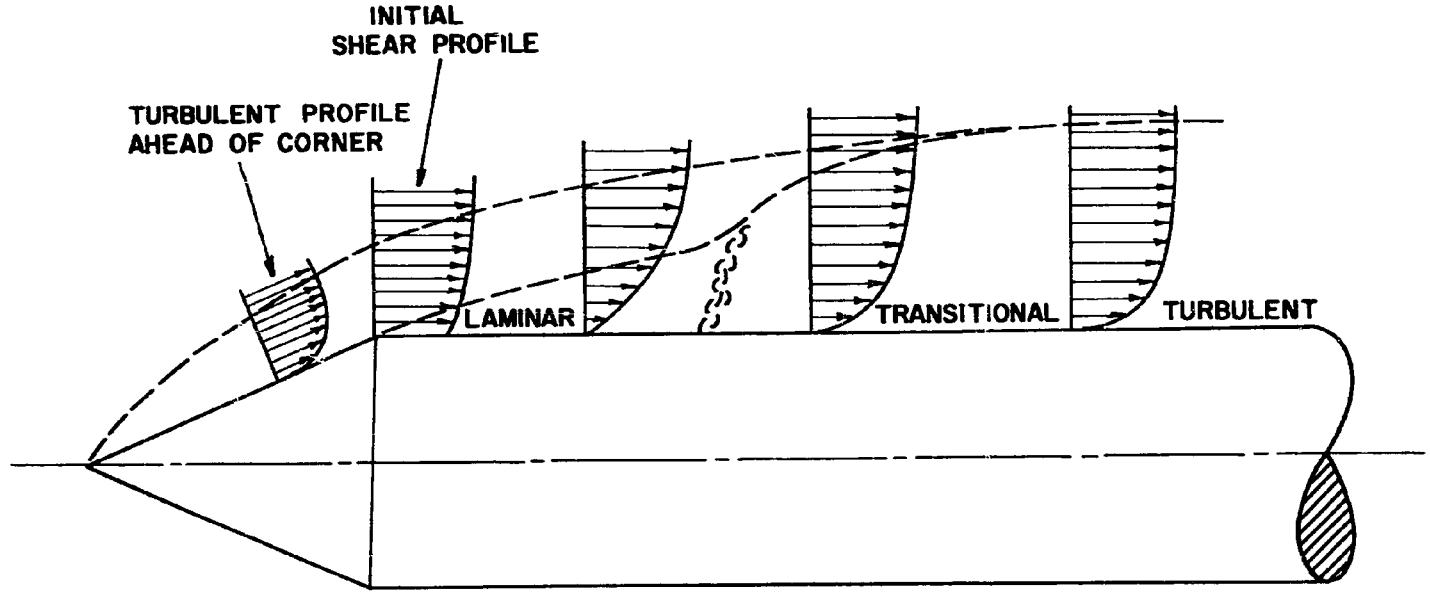

FIG. 1 SCHEME FOR ANALYZING CORNER, TURBULENT AHEAD OF CORNER.

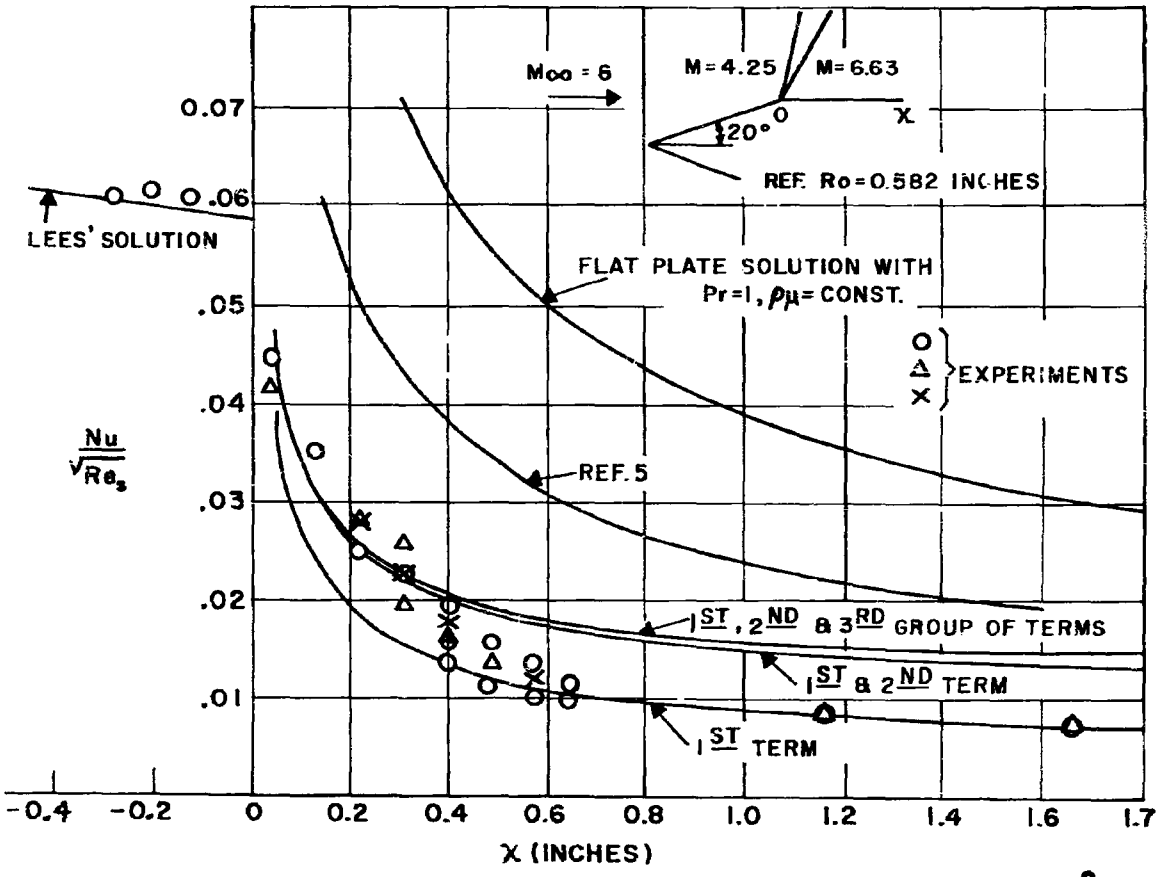

FIG.2 LAMINAR HEAT TRANSFER DISTRIBUTION FOR A 20° SHARP CONE-CYLINDER.

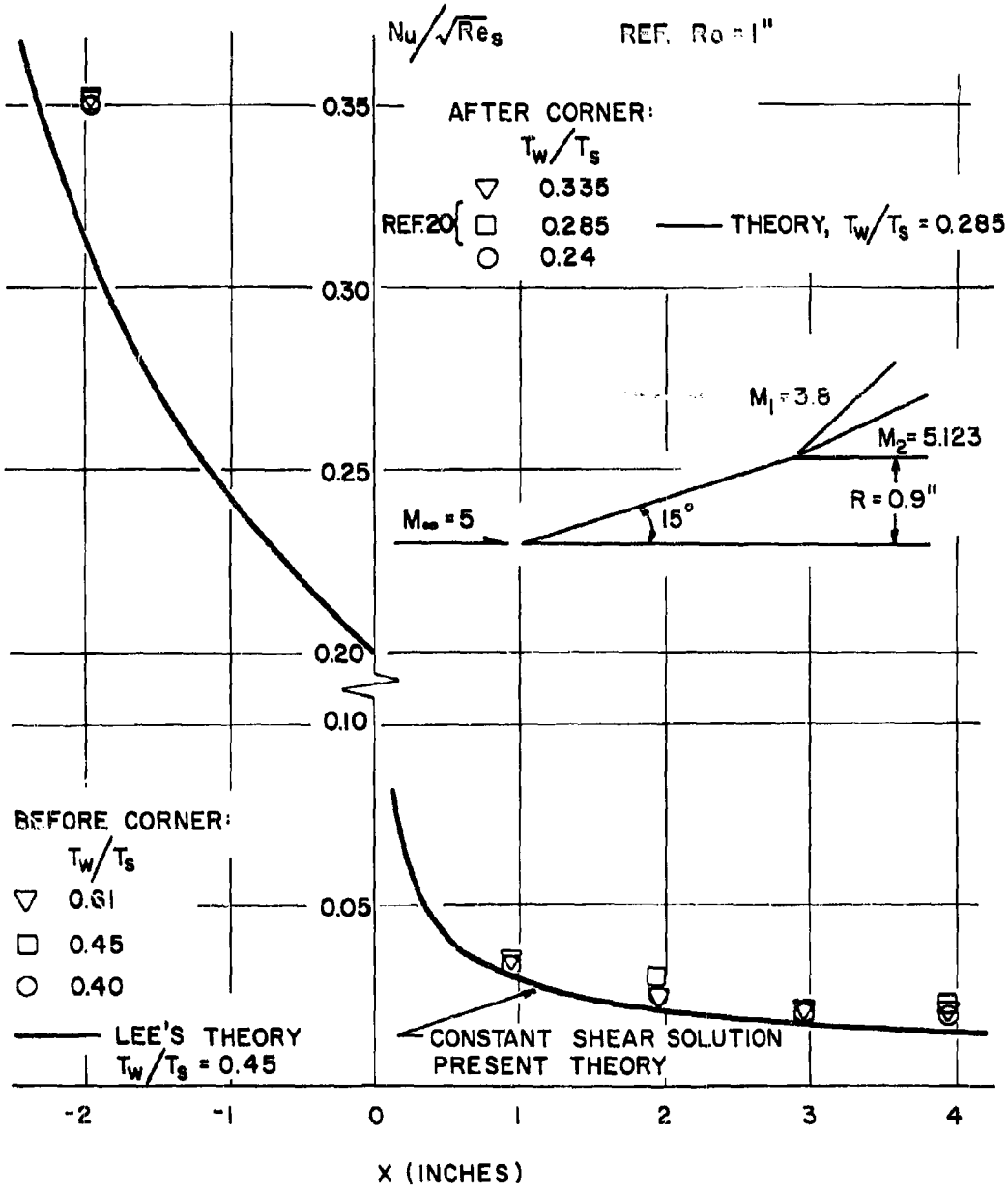

FIG. 3 LAMINAR HEAT TRANSFER DISTRIBUTION FOR A 15° SHARP CONE – CYLINDER.

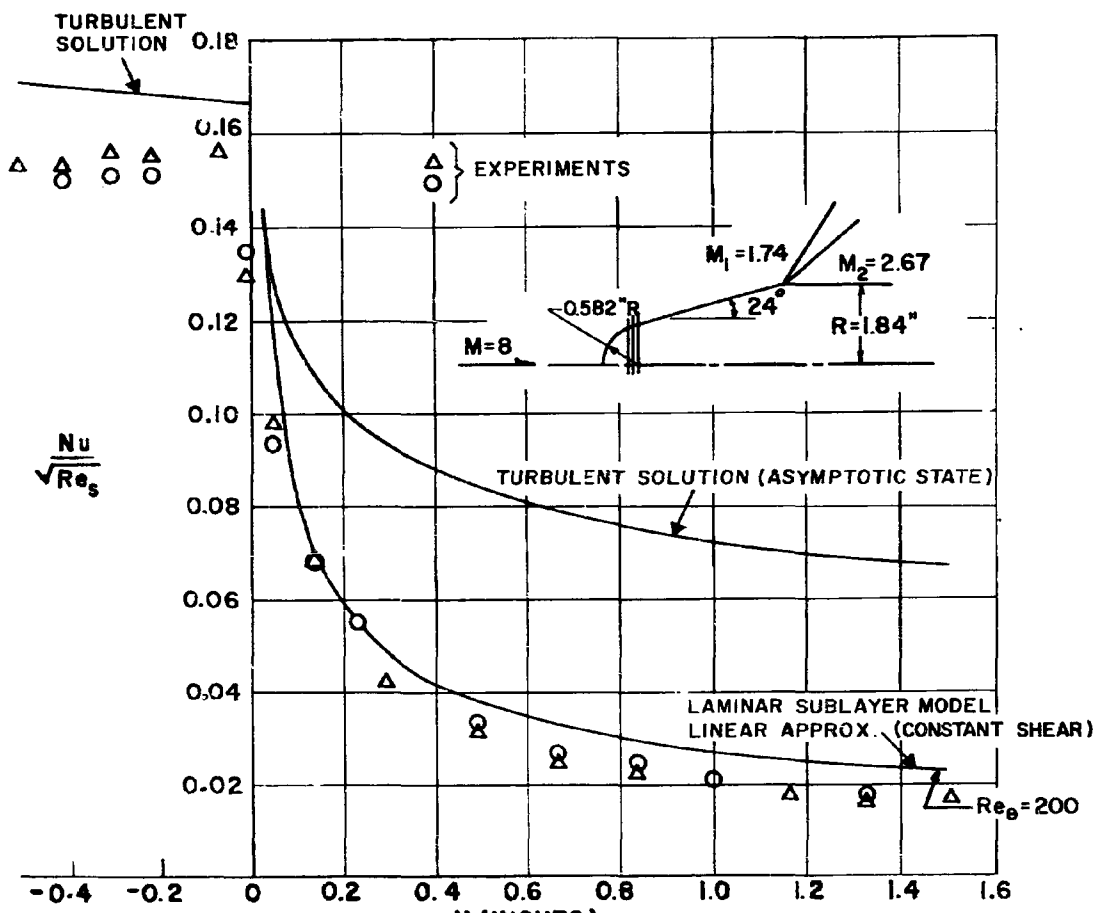

FIG. 4 HEAT TRANSFER DISTRIBUTION FOR A 24° BLUNTED CONE-CYLINDER.

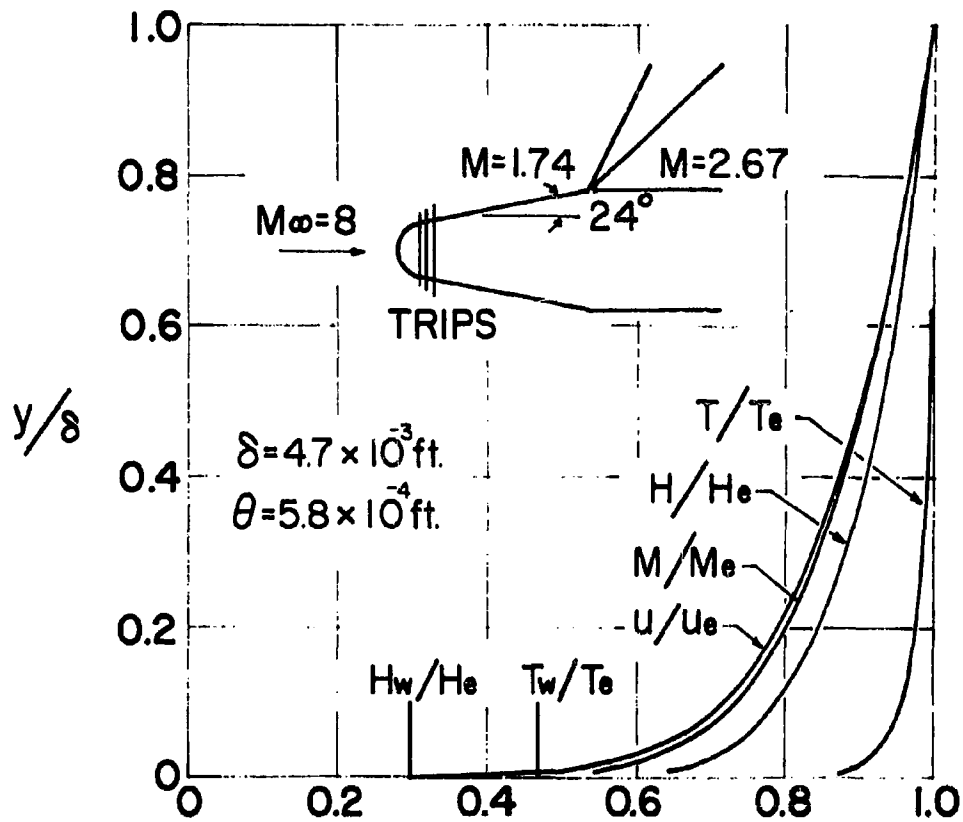

FIG. 4a TURBULENT BOUNDARY LAYER PROFILES BEFORE EXPANSION FOR A 24° BLUNTED CONE-CYLINDER.

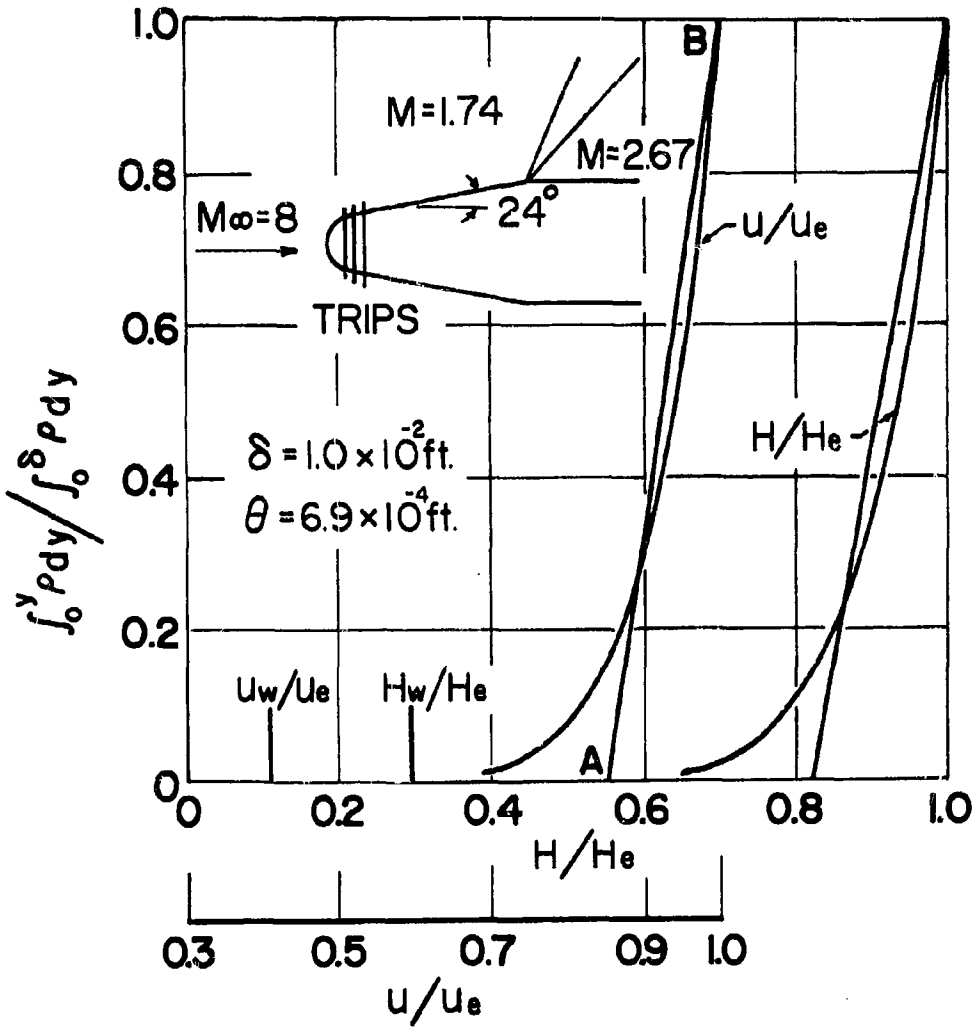

FIG. 4b TURBULENT BOUNDARY LAYER PROFILES AFTER EXPANSION FOR A 24° BLUNTED CONE - CYLINDER.

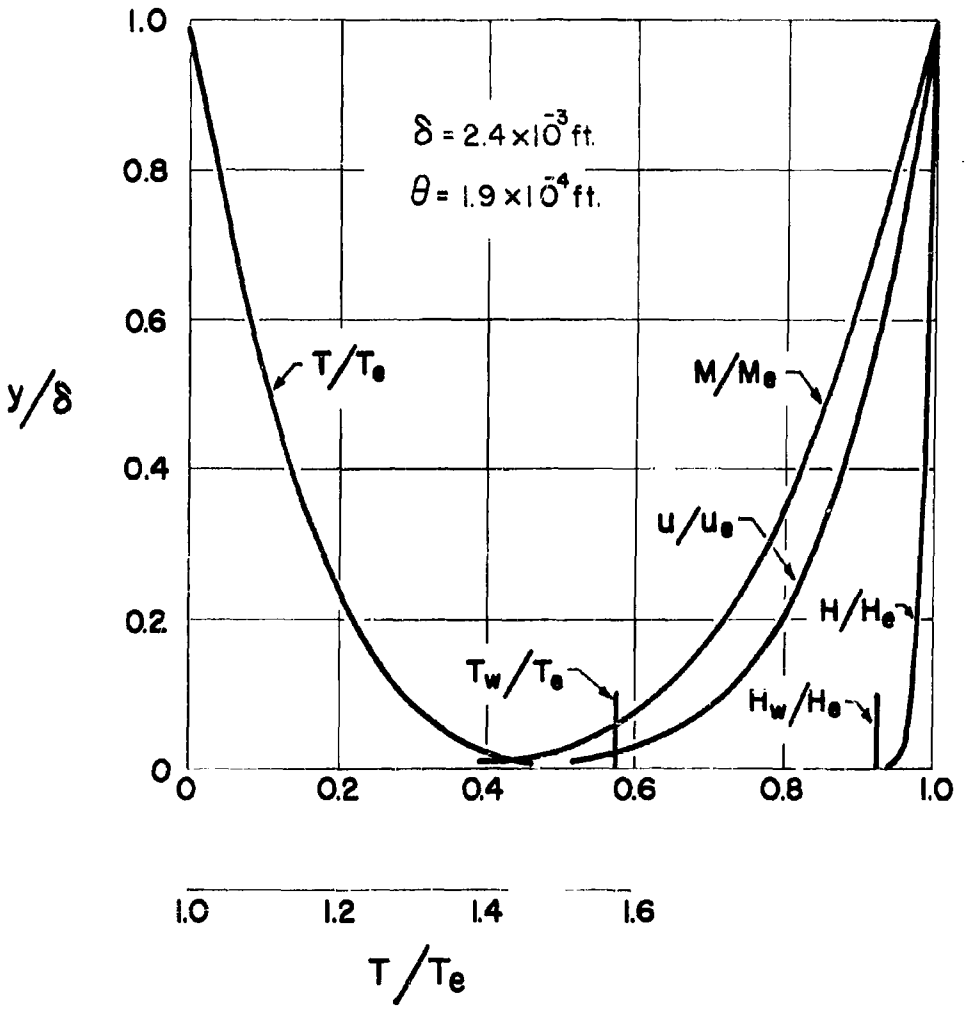

FIG. 5a TURBULENT BOUNDARY LAYER PROFILES BEFORE EXPANSION FOR A 15° BLUNTED CONE-CYLINDER.

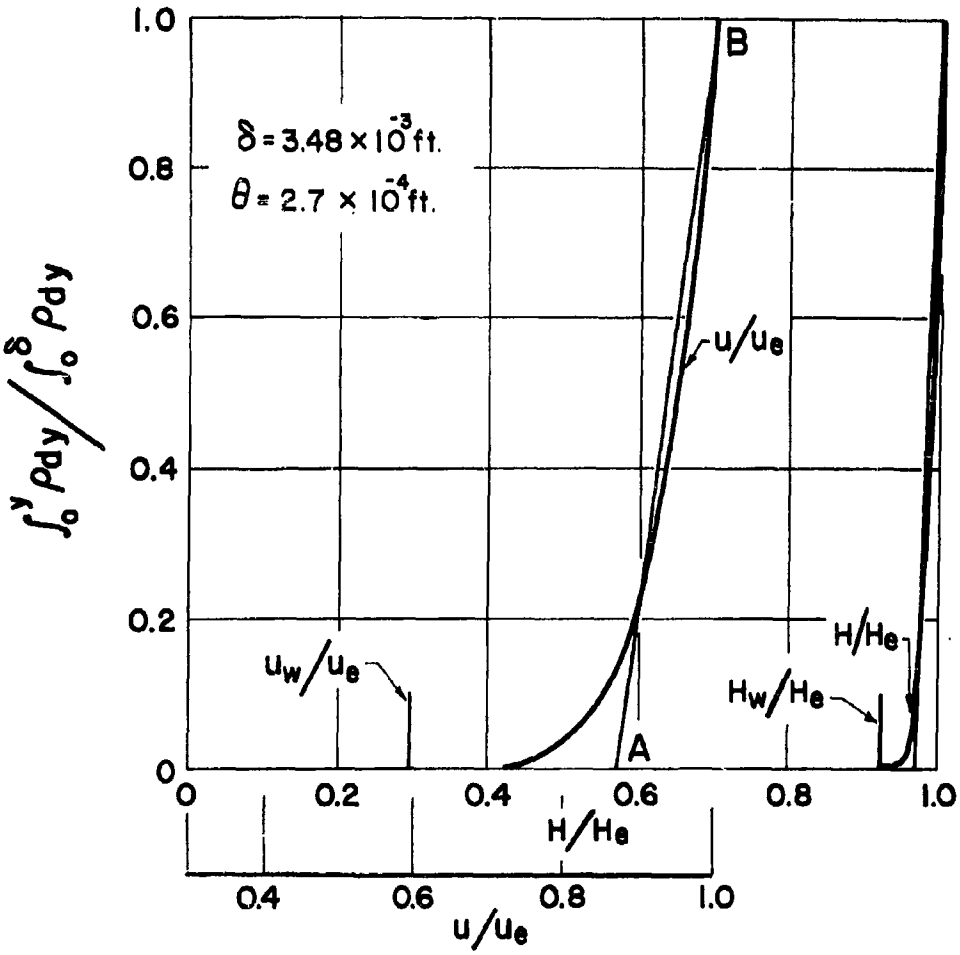

FIG. 5b TURBULENT BOUNDARY LAYER PROFILES AFTER EXPANSION FOR A 15° BLUNTED CONE – CYLINDER.

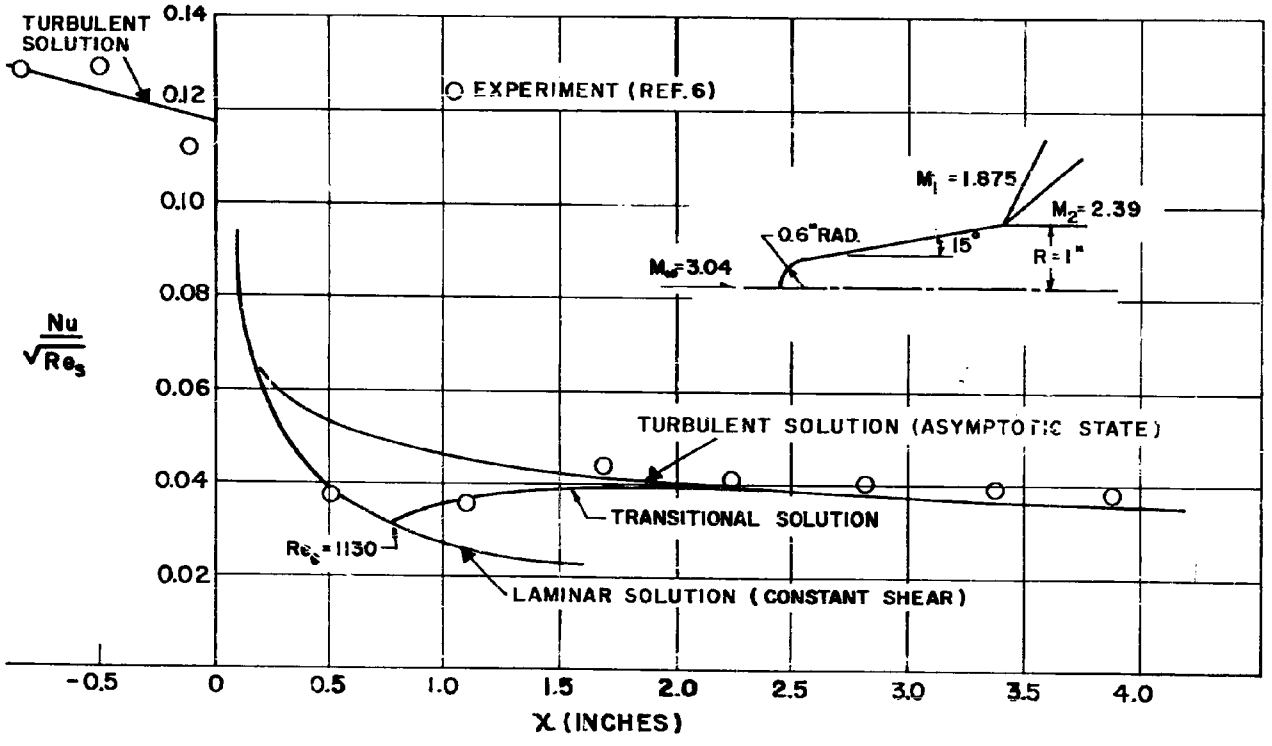

FIG. 6 HEAT TRANSFER DISTRIBUTION FOR A 15° BLUNTED CONE–CYLINDER.

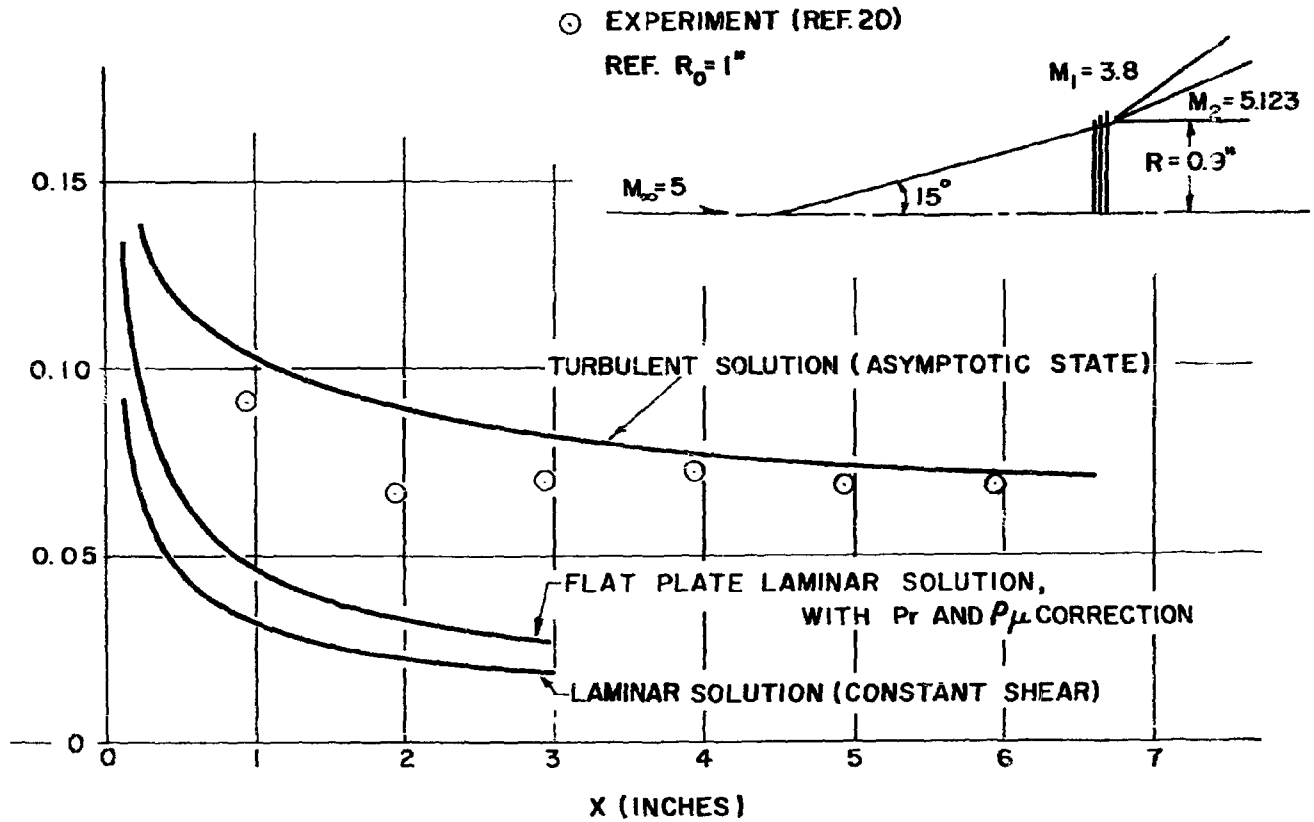

FIG. 7 HEAT TRANSFER DISTRIBUTION FOR A 15° SHARP CONE – CYLINDER.

Bibliographical Control Sheet

1. Originating agency and/or monitoring agency:
   O. A.: Polytechnic Institute of Brooklyn, Brooklyn, New York
   M. A.: Mechanics Division, Air Force Office of Scientific Research
2. Originating agency and/or monitoring agency report number:
   O. A.: PIBAL Report No. 771
   M. A.: None
3. Title and classification of title: LAMINAR, TRANSITIONAL, AND TURBULENT HEAT TRANSFER AFTER A SHARP DISCONTINUITY (UNCLASSIFIED)
4. Personal authors: Victor Zakkay, Kaoru Toba, and Ta-Jin Kuo
5. Date of report: July 1963
6. Pages: 48
7. Illustrative material: 10 figures
8. Prepared for Grant No.: AF-AFOSR-1-63
9. Prepared for Project Code and/or No.: 9781-01
10. Security classification: UNCLASSIFIED
11. Distribution limitations: In accordance with the approved distribution list for unclassified reports.
12. Summary: A flow model has been previously developed for treating the boundary layer characteristics downstream of a surface discontinuity. The flow field in the neighborhood of the discontinuity or a sharp corner is divided into two regions: The flow upstream of the discontinuity which is obtained by standard techniques, and that of downstream which is obtained by expanding both the supersonic and subsonic flow fields upstream of the discontinuity inviscidly around the corner. Downstream of the discontinuity, the flow is represented by a viscous nonsimilar sublayer which starts at the discontinuity, and by a viscous shear layer which has the profiles immediately downstream of the discontinuity as initial conditions. Based upon this flow model, analysis has been developed using the inner and outer expansion techniques.

    It is the purpose of this report to improve on the treatment of the laminar analysis, and to extend the technique of application of this model to include turbulent and transitional flow downstream of the corner. Finally, the results are compared with some of the experimental data available in the literature. It is indicated that good agreement was obtained.